NANO LETTERS
Letter
Cite This: Nano Lett. 2019, 19, 5070−5076
pubs.acs.org/NanoLett

Probing Far-Infrared Surface Phonon Polaritons in Semiconductor Nanostructures at Nanoscale

Ruishi Qi,[†] Renfei Wang,[†] Yuehui Li,[†] Yuanwei Sun,[†] Shulin Chen,[†] Bo Han,[†] Ning Li,[†] Qing Zhang,[‡] Xinfeng Liu,[§] Dapeng Yu,[∥] and Peng Gao*[,†,⊥]

[†]International Center for Quantum Materials, and Electron Microscopy Laboratory, School of Physics and [‡]Department of Materials Science and Engineering, College of Engineering, Peking University, Beijing 100871, China

[§]Division of Nanophotonics, CAS Key Laboratory of Standardization and Measurement for Nanotechnology, CAS Center for Excellence in Nanoscience, National Center for Nanoscience and Technology, Beijing 100190, China

[∥]Shenzhen Key Laboratory of Quantum Science and Engineering, Shenzhen 518055, China

[⊥]Collaborative Innovation Center of Quantum Matter, and Beijing Key Laboratory of Quantum Devices, Beijing 100871, China

S *Supporting Information*

ABSTRACT: Phonon polaritons hold potential prospects of nanophotonic applications at the mid- and far-infrared wavelengths. However, their experimental investigation in the far-infrared range has long been a technical challenge due to the lack of suitable light sources and detectors. To obviate these difficulties, here we use an electron probe with sub-10 meV energy resolution and subnanometer spatial resolution to study far-infrared surface phonon polaritons (~50−70 meV) in ZnO nanostructures. We observe ultraslow propagation and interference fringes of propagating surface phonon polaritons and obtain their dispersion relation through measurements in the coordinate space. By mapping localized modes in nanowires and flakes, we reveal their localized nature and investigate geometry and size effects. Associated with simulation, we show that surface phonon polariton behaviors can be well described by the local continuum dielectric model. Our work paves the way for spatial-resolved investigation of surface phonon polaritons by electron probes and forwards polaritonics in the far-infrared range.

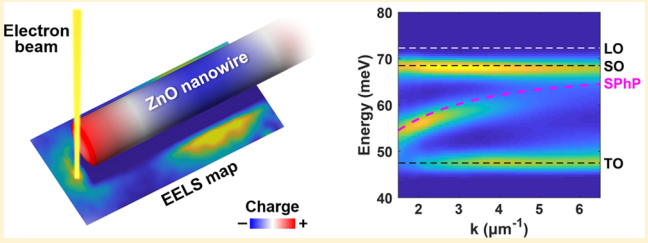

KEYWORDS: *Surface phonon polariton, EELS, STEM, zinc oxide, far-infrared, nanophotonics*

Surface phonon polaritons (SPhPs)[1] are highly desirable to extend numerous plasmonic applications in the visible and near-infrared (IR) range facilitated by surface plasmon polaritons (SPPs) to lower frequencies and to open up unachievable opportunities such as microscopy[2] and data storage.[3] Commonly there are two categories of SPhP modes, that is, propagating SPhPs that are able to propagate along the surface, and localized surface phonon polaritons (LSPhs) confined to subwavelength vicinity of the surface.[1] Although many theoretical and numerical works have been done and potential applications of both types have been anticipated in the past decades,[4−6] their low energy and fine spatial distribution impose stringent requirement on both energy and spatial resolution, making experimental study technically challenging. On the basis of scattering-type scanning near-field optical microscopy (*s*-SNOM), recent researches have revealed the nature of mid-IR SPhPs (e.g., in h-BN, SiC, and MoO_3) with ~20 nm in spatial resolution.[7−11] Despite these great advances, *s*-SNOM is generally limited to two narrow spectral ranges, that is, the near- to mid-IR range (>70 meV) and the terahertz range (<10 meV).[12] However, in most of polar materials SPhPs lie in the far-IR range between them. To date, they have received surprisingly rare investigation due to the unavailability of suitable light sources and detectors, and no detailed spatially resolved study in this range has been reported to the best of our knowledge, hindering our understanding of their nature.

Using swift electron beam, imaging with nanoscale spatial resolution is routine in electron microscopes. However, to detect SPhPs via an electron probe the swift electrons must be strictly monochromated, otherwise the tiny energy loss associated with the excitation of SPhPs will be overwhelmed by the strong background caused by zero loss peak (ZLP). Recent advances of scanning transmission electron microscopes (STEM) enable an atom-wide kiloelectronvolt electron probe with a sub-10 meV energy resolution and atomic spatial resolution, which can transfer energy to materials in various ways, allowing atomically resolved electron energy loss spectroscopy (EELS) analysis of many physical excitations[13−23] in an extremely wide continuous spectral range. Recently, the possibility to probe lattice vibrations using STEM-EELS has been demonstrated.[13,23] Apart from the advantage in spectral range, subnanometer spatial resolution in this technique allows

Received: April 2, 2019
Revised: July 14, 2019
Published: July 19, 2019

DOI: 10.1021/acs.nanolett.9b01350
Nano Lett. 2019, 19, 5070−5076

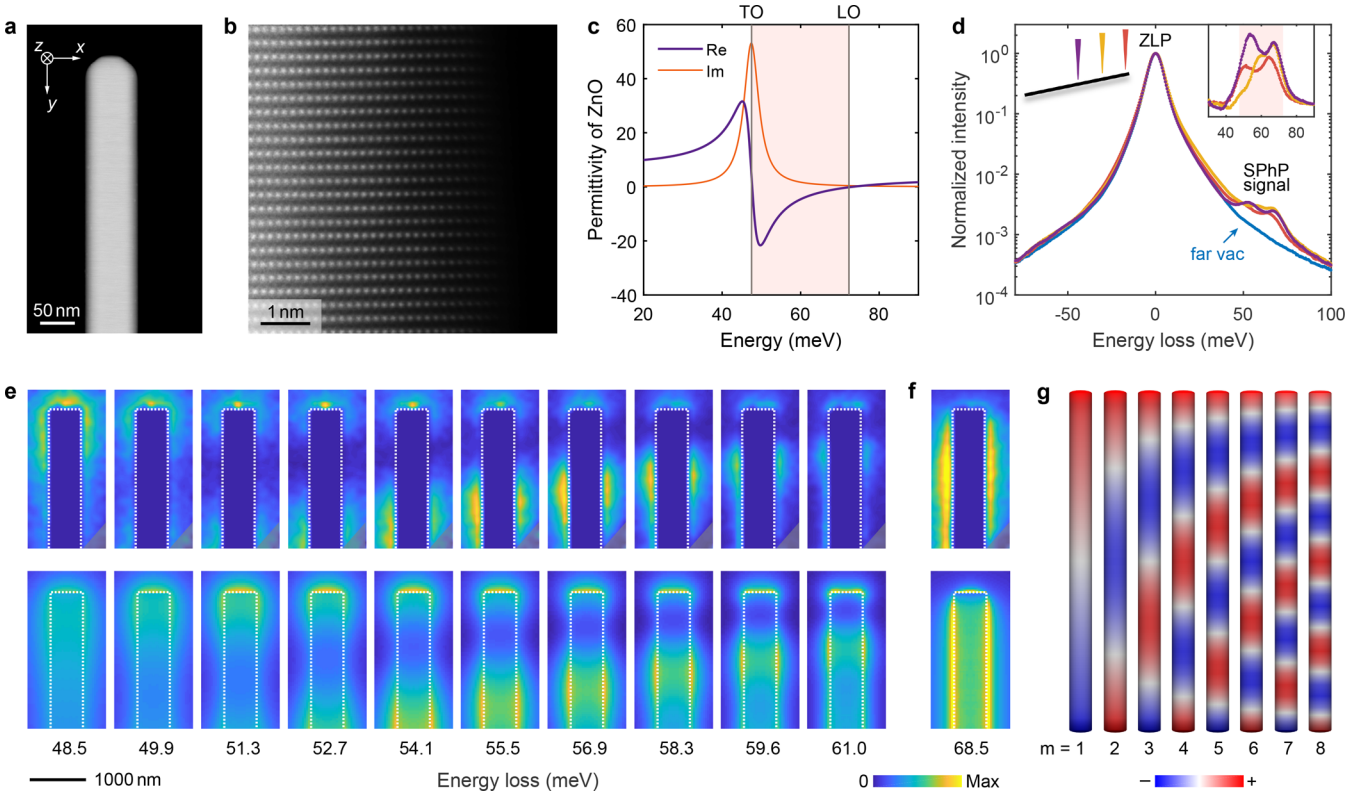

Figure 1. EELS measurements of SPhPs in a single ZnO nanowire. (a) HAADF image of a terminal of a typical ZnO nanowire. (b) Enlarged HAADF image acquired at an edge of a nanowire, viewing along the [210] direction. Each bright spot represents a column of zinc atoms. (c) Complex permittivity of ZnO. Two vertical solid lines mark the energy of TO and LO phonons. The light pink shadow marks the *Reststrahlen* band, where the real part of the permittivity is negative. (d) Typical EEL spectra acquired with an electron beam located at different positions. Maxima of all the spectra are normalized to 1. Blue is beam located in vacuum far from ZnO (about 5 μm) to avoid interaction. Red is beam located in vacuum close to the terminal. Yellow and purple are beams located in vacuum near the nanowire about 1 and 2 μm in distance from the terminal, respectively. See the illustration in the left inset. The right inset shows corresponding background-subtracted spectra, in which the light pink shadow marks the *Reststrahlen* band. (e) Experimental (upper) and simulated (lower) two-dimensional EELS maps near a nanowire with ~570 nm diameter, showing interference fringes of propagating SPhPs of different wavelengths at different energy. (f) Experimental (upper) and simulated (lower) EELS maps associated with LSPhs. White dotted boxes outline the nanowire. This nanowire is supported by an amorphous carbon grid (Figure S1d in Supporting Information), which blocked the signal in a small region near the bottom right corner (triangular gray shadow) in the experimental maps in (e,f). (g) Simulated surface charge distribution of several eigenmodes of the lowest orders. The diameter of the nanowire is the same as that in (e,f) and the length is set 8 μm.

us to study fine spatial distribution of SPhPs in tiny nanostructures.

In this work, we use an electron probe of 8 meV energy resolution based on a Nion UltraSTEM 200 microscope with monochromator and aberration corrector to study both propagating and localized SPhPs in ZnO nanowires and flakes. Aided by and in good agreement with numerical simulation, our experiment verifies previous theoretical works. We excite and probe SPhPs in the far-IR range at nanoscale in individual ZnO nanowires and flakes and show the applicability of the local continuum dielectric model (LCDM).[5,24] We observe ultraslow propagation of propagating SPhPs in a single nanowire and reflection at a terminal leading to interference fringes. We also map the spatial distribution of LSPhs in ZnO nanowires and flakes and reveal their energy dependence on size. These results can help us to understand SPhP behaviors in nanostructures and provides useful information for nanophotonic applications in the far-IR range. Filling the gap between the mid-IR and the terahertz range, monochromatic STEM-EELS is complementary for *s*-SNOM technique, providing unprecedented opportunities to uncover light-matter interactions at nanoscale.

Figure 1a shows a high-angle annular dark-field (HAADF) image of a typical ZnO nanowire acquired with an electron beam traveling along the *z*-direction. The crystal structure of ZnO is confirmed to be wurtzite based on electron diffraction patterns (Figure S1 in Supporting Information). For clarity, we set *y*-axis along the nanowire ([001] direction) and $y = 0$ at the terminal. Figure 1b is an atomically resolved HAADF image acquired at an edge of a nanowire projecting along the [210] direction in which each bright spot represents a column of zinc atoms.

Figure 1c shows the complex permittivity ϵ of ZnO. The energy band between the energy of transverse optical (TO, 47.5 meV) and longitudinal optical (LO, 72.3 meV) phonons is called the *Reststrahlen* band[1] (light pink shadow) within which the real part of the permittivity is negative and thus SPhP modes can be sustained. In our experiment, Figure 1d shows typical EEL spectra acquired with the electron beam located at different positions. The spectrum in blue is acquired in a vacuum region far from the specimen, showing a sharp ZLP with no signal obtained. The full width at half-maximum of the ZLP defines the energy resolution, which in our experiment is about 8 meV, enabling us to detect SPhPs. The spectra in red, yellow, and purple are acquired in vacuum in the vicinity of different

DOI: 10.1021/acs.nanolett.9b01350
Nano Lett. 2019, 19, 5070−5076

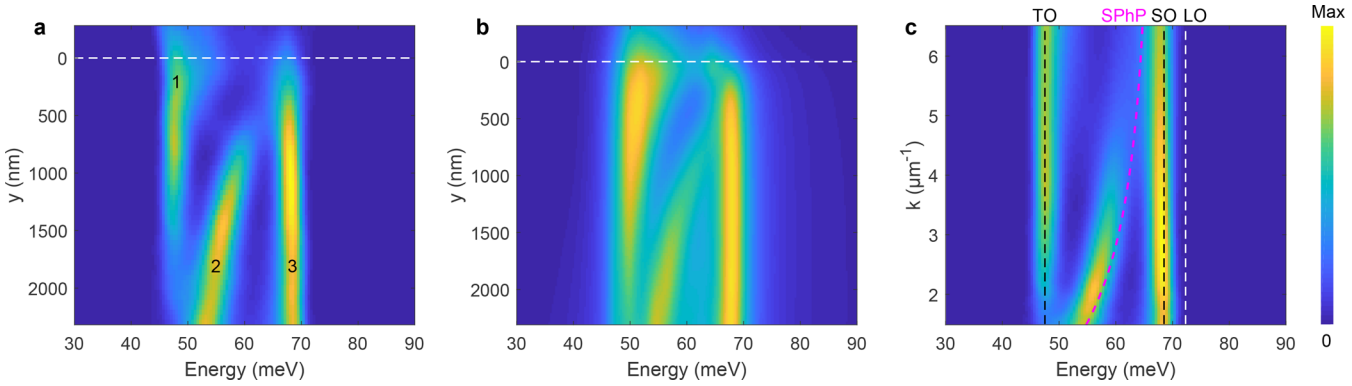

Figure 2. Measuring the dispersion relation of SPhPs in the coordinate space. (a) Experimental EEL spectra as a function of the location of the electron beam. Horizontal axis stands for energy loss of the swift electron and the loss intensity is shown by color. Vertical axis y denotes the position of the electron beam, expressed by the distance to the terminal (marked by the white dashed line) of the nanowire. (b) Simulation results for (a) using boundary element method. (c) Experimental EEL spectra as a function of the wavenumber $k = \pi/y$ of the SPhP. Magenta dashed line is the dispersion relation of the fundamental TM mode calculated by eq 1 in the main text, and vertical dashed lines mark the energy of TO, SO, and LO phonons.

positions of a nanowire (see the left inset in Figure 1d) and the right inset shows corresponding background-subtracted spectra. In the *Reststrahlen* band, we find resonant peaks that resulted from the coupling between the swift electrons and SPhP modes excited by the beam. With the beam located at different positions, the energy and intensity of the peaks are different.

Note that the signal of SPhPs is more intense in thick nanowires, allowing better signal-to-noise ratios. However, due to intense interaction with ZnO most electrons are absorbed when traveling in thick nanowires, preventing us from acquiring any signal. Fortunately, when the electron beam passes near the nanowire without intersecting it (aloof mode) SPhPs can still be excited and well detected due to the long-range Coulomb interaction, and much information can be obtained from the spectra recorded in aloof mode. For a nanowire with a diameter of 570 nm and sufficiently long (on the order 10 μm), upper panels in Figure 1e depict experimental two-dimensional EELS maps at different energy. To corroborate our experimental results, we performed boundary element method (BEM) simulation,[25] solving Maxwell's equations based on LCDM. Simulated two-dimensional EELS maps at corresponding energy are shown in lower panels in Figure 1e. The agreement between the experiment and simulation confirms the effectiveness of LCDM theory in describing SPhPs in the far-IR range. In each panel, the SPhP signal is intense near the terminal, and another antinode appears in the lower region. Such nodal patterns can be interpreted as interference fringes of propagating SPhPs. After being excited by the electron beam, SPhPs propagate along the nanowire and are reflected at the terminal, giving birth to interference fringes resembling a standing wave. At higher energy with the wavelength reduced, the distance between the two antinodes decreases correspondingly. These results are similar to *s*-SNOM measurements of mid-IR SPhP behaviors in one-dimensional h-BN nanotubes[11] and nanowires[26] and EELS measurements of SPPs in metallic nanowires in the visible range.[27]

For a finite-long nanowire, simulated surface charge distributions associated with several lowest-order eigenmodes are illustrated in Figure 1g. With m denoting the number of nodes, $m = 1$ correspondes to the dipolar mode in which the charge is concentrated at two terminals. For modes with higher m, the interference leads to an alternate distribution of positive and negative surface charge density. In our experiment, the nanowire is long enough to be treated as semi-infinite in which these modes become continuous, as shown in Figure 1e.

We also observe an LSPh mode at about 68.5 meV. Unlike propagating SPhPs, LSPhs do not propagate along the surface but are localized to the vicinity of the surface. For an infinite cylinder, theoretical analysis (see Supporting Information) predicts a polaritonic eigenmode at the energy of surface optical (SO) phonon ω_{so} such that $\mathrm{Re}[\varepsilon(\omega_{so})] = -1$, which for ZnO gives out the energy 68.5 meV. Figure 1f shows the experimental and simulated EELS maps of this mode. As expected, this mode is intense at the surface and shows an exponential-like decay as the beam moves toward either inside or outside. From the experimental result, its decrease on the vacuum side[18] can be verified though the decay inside the nanowire which is not detected due to the low signal.

For quantitative analysis, Figure 2a is a line profile of the experimental data shown in Figure 1e along the y-direction, summing up spectra along the x-axis, and Figure 2b is the corresponding simulation result. Three peaks are observed, that is, two peaks (1 and 2) corresponding to propagating SPhPs and one peak (3) of LSPhs. Peak 1 at ~48 meV is intense near the terminal, which mainly results from the dipolar mode of the nanowire. For a sufficiently long nanowire, as the wavevector of the dipolar mode approaches zero, its energy aproaches the TO energy, which is in aggrement with our experiment. At the terminal, the energy of this peak shows a slight blueshift behavior as well as becoming broader in width, which should be attributed to the fact that all the SPhP eigenmodes shown in Figure 1g are intense in the vicinity of the terminal. As verified by previous experimental works in SPPs,[27] the reflection phase shifts for multipolar modes approach zero quickly with increasing order m, leading to a constructive interference near the terminal. The contributions from the dipolar and the multipolar modes are mixed into one broad peak, making its energy higher near the terminal (for further illustration, see Figure S4 and related text in Supporting Information).

Peak 2 exhibits a prominent blueshift behavior near the terminal, which can be better understood by referring to the dispersion relation $\omega = \omega(k)$. From Maxwell's equations one can derive the dispersion relation of SPhPs with no azimuthal variation (the fundamental TM mode) in an infinitely long cylinder[28,29]

DOI: 10.1021/acs.nanolett.9b01350
Nano Lett. 2019, 19, 5070−5076

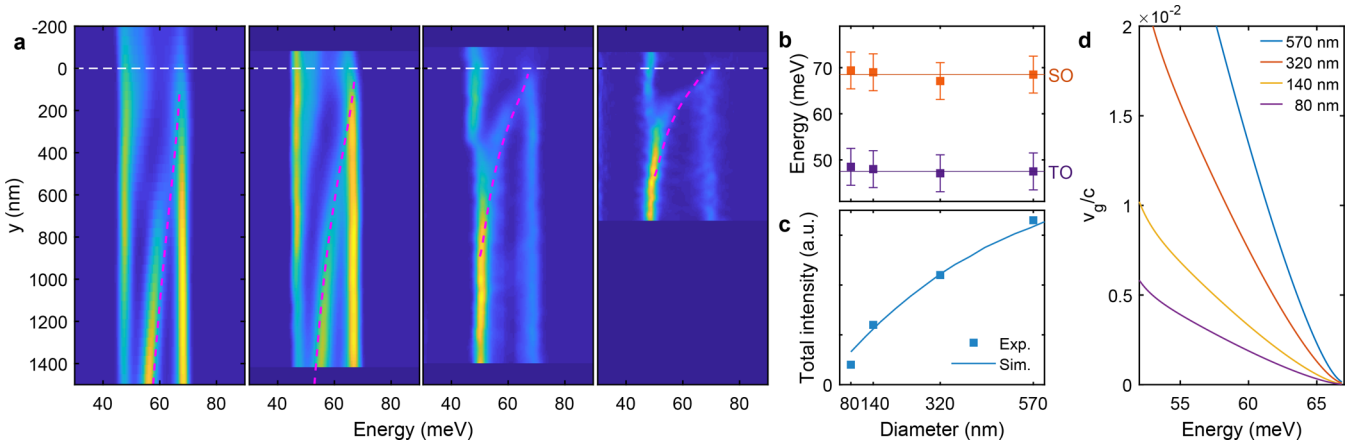

Figure 3. Size effects of SPhPs in ZnO nanowires. (a) EELS as a function of the location of the electron beam y in nanowires of different diameters d. d = 570, 320, 140, and 80 nm from left to right. Horizontal white dashed lines mark the terminal. Magenta dashed lines are calculated by eq 1 in the main text. (b) The upper and lower limits of the energy of SPhPs. Solid squares with error bars present the experimental energy of the dipolar mode and the LSPh, whereas the energy of TO and SO phonon are marked by solid lines. (c) Normalized total energy loss intensity with beam located at the immediate vicinity of the nanowire. (d) Calculated group velocity of propagating SPhPs in nanowires.

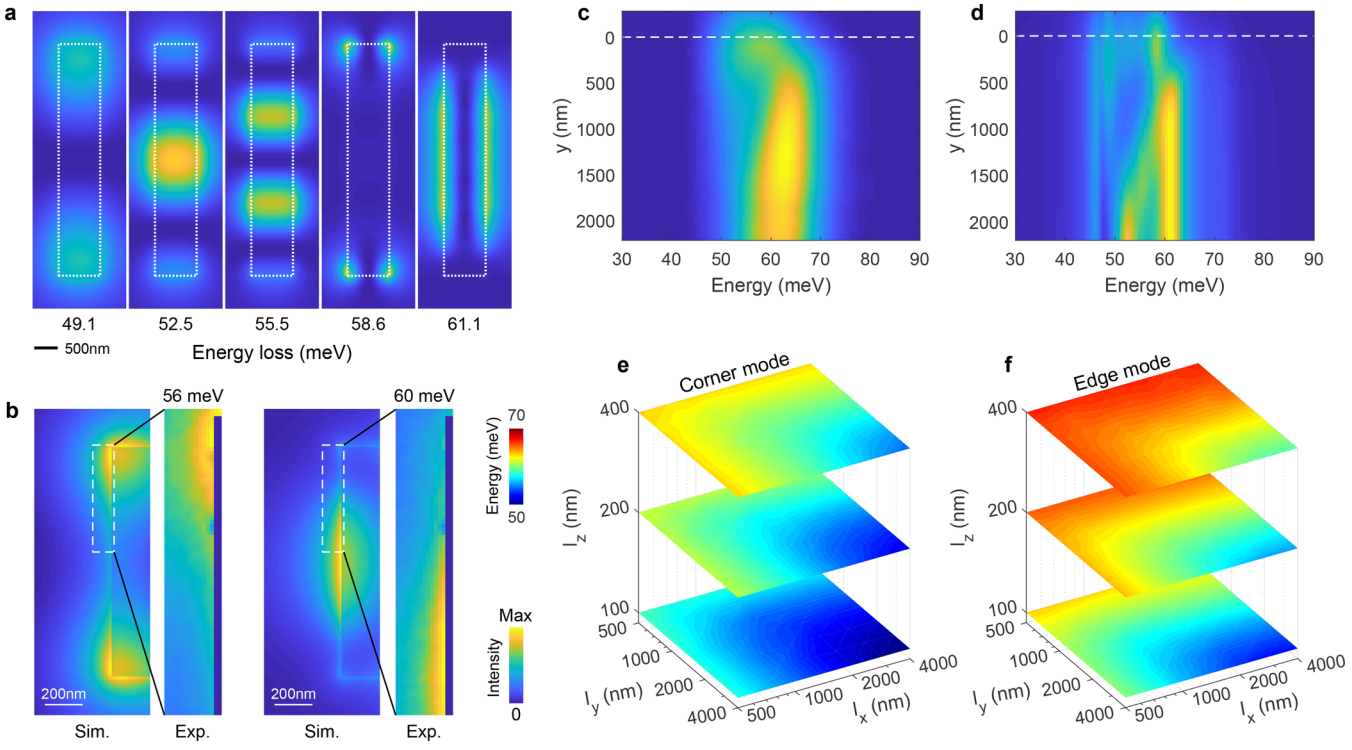

Figure 4. SPhP modes in ZnO flakes. (a) Simulated EELS maps of different resonant modes in a 5000 × 900 × 240 nm ZnO flake. Modes in the first three panels show the interference fringes of propagating SPhPs in long narrow flakes. The last two panels show the corner mode and the edge mode, respectively. Dotted boxes outline the flake. (b) Simulated and experimental EELS maps of the corner mode at 56 meV and the edge mode at 60 meV in a 3600 × 1200 × 120 nm flake. White dashed boxes in simulated maps show the area corresponding to the experimental maps. (c,d) Experimental and simulated EELS as a function of the location of the electron beam for the flake in (a). Colorbars in (a−d) represent loss intensity. (e,f) Simulated energy of the corner mode and the edge mode (distributing along y-direction) in flakes with various size. Three axes represent l_x, l_y ,and l_z respectively, and the energy of both modes is shown by color.

$$\nu'\epsilon\frac{\mathrm{d}\ln I_0(\nu r)}{\mathrm{d}(\nu r)} - \nu\frac{\mathrm{d}\ln K_0(\nu' r)}{\mathrm{d}(\nu' r)} = 0 \qquad (1)$$

where $\epsilon = \epsilon(\omega)$ is the permittivity of ZnO, r stands for the radius of the nanowire, $\nu \equiv \sqrt{k^2 - \epsilon\omega^2/c^2}$, $\nu' \equiv \sqrt{k^2 - \omega^2/c^2}$, k is the wavenumber, ω is the vibrational frequency, c is the speed of light in vacuum, and functions I_0 and K_0 are the modified Bessel functions of the first and second kind of order zero. In Figure 2c, the magenta dashed line is the calculation result. The energy of SPhPs at k = 0 equals TO energy and becomes higher with increasing k, approaching ω_{so} asymptotically. Assuming zero reflection phase shift, antinodes always appear at both the terminal and near the electron beam. Therefore, the distance between them approximately equals a half wavelength π/k (or its integer multiple but the former case predominates so the latter is negligible). In other words, the part of the nanowire between the

DOI: 10.1021/acs.nanolett.9b01350
Nano Lett. 2019, 19, 5070−5076

beam and the terminal serves as an optical cavity, selecting SPhP modes with certain wavelengths. As the beam moves closer to the terminal, SPhPs of higher wavenumber k are excited, resulting in an increase in its energy. Thus, we can obtain the dispersion relation experimentally from data shown in Figure 2a. To illustrate this, we replot Figure 2a as Figure 2c, showing spectra as a function of $k = \pi/y$. The result agrees relatively well with eq 1 (magenta dashed line), whereas the small deviation is likely due to inaccuracy in $k = \pi/y$, which may result from nonzero reflection phase shifts. The sensitivity of the transformed π/y at small y-values may also lead to inaccuracy at large k-values. Additionally, at higher energy the signal of propagating SPhPs becomes less intense, indicating a weaker coupling between the electron beam and propagating SPhPs of higher wavenumber.[30]

Now we focus on size effects of SPhP modes. In Figure 3a, we compare SPhP behaviors in four nanowires with diameters of 570, 320, 140, and 80 nm. The most evident difference among the four nanowires is the characteristic spatial scale of the energy shift. Derived from eq 1, in our case ω as a function of kr remains approximately the same for nanowires with different r, as shown as magenta dashed lines in each panel. Thus, theoretically the characteristic spatial scale of energy shift is proportional to r, which is confirmed by our experiment. Figure 3b shows that the lower and upper limits of the energy of SPhPs, as predicted to be the energy of TO (47.5 meV) and SO (68.5 meV) phonons, remain almost constant in different nanowires. In addition, as shown in Figure 3c, the total energy loss intensity becomes weaker as the diameter decreases, indicating lower exciting efficiency due to a decreased volume of the electromagnetic field in smaller nanostructures.

On the basis of calculated dispersion relation in these nanowires, we plot the group velocity ($v_g = d\omega/dk$) of propagating SPhPs in Figure 3d. At higher energy, the exceptional low slopes of the dispersion relation lead to remarkably small group velocities, especially in thin nanowires. Theoretically, infinitesimal v_g can be achieved at energy near that of SO phonons, for example, $v_g = 10^{-5}c$ at 67 meV in the 80 nm nanowire, but practically in such conditions the excitation efficiency is too low. Nonetheless, for the thick nanowire with 570 nm diameter, $1.3 \times 10^{-2}c$ at 60 meV can still be achieved with an acceptable excitation efficiency, which is comparable to that of ultraslow polaritons reported in h-BN[31,32] and MoO_3[8] and could be utilized to create slow light in a simple way.[33]

Interestingly, although SPhP modes depend a lot on the geometry of the nanoparticle, in a wirelike flake whose length l_y is far greater than the width l_x and thickness l_z, SPhPs' behavior is largely like that in a nanowire mentioned above. Figure 4a shows our simulation results for a $5000 \times 900 \times 240$ nm flake. Modes in the first three panels resembling those corresponding modes in Figure 1e reveal the commonality of SPhP propagation behaviors in wirelike structures, regardless of the shape of their cross section. This reflects the nature of SPhP in quasi-one-dimensional systems caused by reflection at the boundaries and the subsequent interference.

Compared with genuine nanowires, the major difference of this wirelike flake lies in the resonance of LSPh modes, including the corner mode at 58.6 meV and the edge mode at 61.1 meV, similar to those in finite size cubes.[34,35] These LSPh modes only appear around sharp corners and edges of the nanoparticle while being absent in a cylinder-shaped nanowire, which is in agreement with theoretical[5] and experimental results[23] in other materials. We acquire EELS maps of the corner mode and the edge mode in a $1200 \times 3600 \times 120$ nm flake (the thickness is calculated using log-ratio technique[36]) in which the difference in energy between the edge mode and the corner mode is larger, as shown in Figure 4b. The spatial distribution of both modes is in good agreement with the simulation presented in the left side of the corresponding experimental map.

For the former flake, Figure 4c,d shows the experimental (not deconvoluted, see Section 1 in Supporting Information) and simulated line profiles, respectively, in the same manner as Figure 2a,b. Insufficient energy resolution prevents us from experimentally distinguishing different peaks in Figure 4d. Yet if we convolute the simulated spectra with an 8 meV Gaussian peak, the result agrees well with Figure 4c (see Figure S5 and related text in Supporting Information).

For further investigation, Figure 4e,f presents the simulated energy of the edge mode and the corner mode in rectangular flakes of different sizes. The energy of the two modes varies similarly with the size of flakes, though in general the edge mode has a higher energy. As the thickness l_z increases, the vibrational energy becomes higher, which can be attributed to the reduced coupling between the upper and lower surfaces.[18,37] On the contrary, the vibrational energy decreases as the length l_y or the width l_x increases.

Finally, we briefly discuss the advantages of probing SPhPs via STEM-EELS technique and current insufficiencies that should be addressed in the future. First, without the need of laser sources the extremely wide accessible spectra range makes STEM-EELS technique applicable to a greater variety of polaritonic materials. Second, the subnanometer spatial resolution facilitates the investigation in tiny nanostructures, such as heterostructure interfaces, defects, and quantum dots. Third, relatively intense interaction between electrons and materials also makes it advantageous in exciting and detecting signals in tiny nanostructures. Fourth, EELS is sensitive to more multipole modes, including optical inactive dark modes.[5,30] However, although our state-of-the-art STEM enables a sub-10 meV energy resolution, it still needs further improvements in order to distinguish resonant peaks close to each other in energy. This should be achievable with the fast development of monochromators and related STEM techniques in the future.

In summary, we excite and probe SPhPs in the far-IR range with an electron probe. We directly map the distribution of propagating SPhPs and LSPhs up to atomic resolution and also obtain the dispersion relation by measurements in the coordinate space. Modes in flakes are also mapped and size effects in both shapes have been illustrated. This information should be useful for understanding SPhP behaviors at nanoscale and for further developing related technologies. Furthermore, the STEM-EELS with atomic spatial resolution and sub-10 meV energy resolution provides new opportunities to explore substantial physical excitations in a wide energy range, including far-IR SPhPs behaviors in nanostructures.

■ ASSOCIATED CONTENT

Supporting Information

The Supporting Information is available free of charge on the ACS Publications website at DOI: 10.1021/acs.nanolett.9b01350.

Information about experimental details, theoretical analysis, and numerical simulation (PDF)

DOI: 10.1021/acs.nanolett.9b01350
Nano Lett. 2019, 19, 5070−5076

AUTHOR INFORMATION

Corresponding Author

*E-mail: p-gao@pku.edu.cn.

ORCID

Qing Zhang: 0000-0002-6869-0381
Xinfeng Liu: 0000-0002-7662-7171
Peng Gao: 0000-0003-0860-5525

Author Contributions

R.Q. and R.W. contributed equally to this work. R.Q., R.W., and P.G. conceived the idea. R.W. prepared the sample. R.W. and R.Q. acquired the EELS data. R.Q. carried out the numerical simulation and performed the data analysis assisted by R.W. Y.S. and Y.L. acquired the atomically resolved HAADF images. S.C. acquired the SEM images. B.H. performed the electron diffraction. Y.L., Y.S., and N.L. helped with the microscope operation. R.Q. finalized the paper. All authors contributed to the work through fruitful discussion and/or comments to the manuscript. P.G. supervised the project.

Notes

The authors declare no competing financial interest.

ACKNOWLEDGMENTS

The work was supported by the National Key R&D Program of China (Grant 2016YFA0300804), the National Natural Science Foundation of China (Grant 51672007, 11874130), National Equipment Program of China (ZDYZ2015-1), and Open Research Fund Program of the State Key Laboratory of Low-dimensional Quantum Physics (KF201904). We gratefully acknowledge the support from the National Program for Thousand Young Talents of China. We also acknowledge Electron Microscopy Laboratory in Peking University for the use of electron microscopes and financial support. We thank Dr. Chenglong Shi and Dr. Tracy Lovejoy for assistance in microscope operation, Prof. Jiandong Guo at the Institute of Physics, and Mr. Ruochen Shi for the inspiring discussion.

REFERENCES

(1) Caldwell, J. D.; Lindsay, L.; Giannini, V.; Vurgaftman, I.; Reinecke, T. L.; Maier, S. A.; Glembocki, O. J. Low-loss, infrared and terahertz nanophotonics using surface phonon polaritons. *Nanophotonics* **2015**, *4*, 44−68.

(2) Taubner, T.; Korobkin, D.; Urzhumov, Y.; Shvets, G.; Hillenbrand, R. Near-field microscopy through a SiC superlens. *Science* **2006**, *313*, 1595.

(3) Ocelic, N.; Hillenbrand, R. Subwavelength-scale tailoring of surface phonon polaritons by focused ion-beam implantation. *Nat. Mater.* **2004**, *3*, 606−9.

(4) Ha, D. T.; Thuy, D. T.; Hoa, V. T.; Van, T. T. T.; Viet, N. A. On the theory of three types of polaritons (phonon, exciton and plasmon polaritons). *J. Phys.: Conf. Ser.* **2017**, *865*, No. 012007.

(5) Lourenço-Martins, H.; Kociak, M. Vibrational surface electron-energy-loss spectroscopy probes confined surface-phonon modes. *Phys. Rev. X* **2017**, *7*, No. 041059.

(6) Gubbin, C. R.; Maier, S. A.; De Liberato, S. Theoretical investigation of phonon polaritons in SiC micropillar resonators. *Phys. Rev. B: Condens. Matter Mater. Phys.* **2017**, *95*, No. 035313.

(7) Atkin, J. M.; Berweger, S.; Jones, A. C.; Raschke, M. B. Nano-optical imaging and spectroscopy of order, phases, and domains in complex solids. *Adv. Phys.* **2012**, *61*, 745−842.

(8) Ma, W.; Alonso-Gonzalez, P.; Li, S.; Nikitin, A. Y.; Yuan, J.; Martin-Sanchez, J.; Taboada-Gutierrez, J.; Amenabar, I.; Li, P.; Velez, S.; Tollan, C.; Dai, Z.; Zhang, Y.; Sriram, S.; Kalantar-Zadeh, K.; Lee, S. T.; Hillenbrand, R.; Bao, Q. In-plane anisotropic and ultra-low-loss polaritons in a natural van der Waals crystal. *Nature* **2018**, *562*, 557−562.

(9) Basov, D. N.; Fogler, M. M.; Garcia de Abajo, F. J. Polaritons in van der Waals materials. *Science* **2016**, *354*, aag1992.

(10) Keilmann, F.; Hillenbrand, R. Near-field microscopy by elastic light scattering from a tip. *Philos. Trans. R. Soc., A* **2004**, *362*, 787−805.

(11) Xu, X. G.; Ghamsari, B. G.; Jiang, J. H.; Gilburd, L.; Andreev, G. O.; Zhi, C.; Bando, Y.; Golberg, D.; Berini, P.; Walker, G. C. One-dimensional surface phonon polaritons in boron nitride nanotubes. *Nat. Commun.* **2014**, *5*, 4782.

(12) Khatib, O.; Bechtel, H. A.; Martin, M. C.; Raschke, M. B.; Carr, G. L. Far infrared synchrotron near-field nanoimaging and nano-spectroscopy. *ACS Photonics* **2018**, *5*, 2773−2779.

(13) Krivanek, O. L.; Lovejoy, T. C.; Dellby, N.; Aoki, T.; Carpenter, R. W.; Rez, P.; Soignard, E.; Zhu, J.; Batson, P. E.; Lagos, M. J.; Egerton, R. F.; Crozier, P. A. Vibrational spectroscopy in the electron microscope. *Nature* **2014**, *514*, 209−12.

(14) Lovejoy, T. C.; Corbin, G. C.; Dellby, N.; Hoffman, M. V.; Krivanek, O. L. Advances in ultra-high energy resolution STEM-EELS. *Microsc. Microanal.* **2018**, *24*, 446−447.

(15) Idrobo, J. C.; Lupini, A. R.; Feng, T.; Unocic, R. R.; Walden, F. S.; Gardiner, D. S.; Lovejoy, T. C.; Dellby, N.; Pantelides, S. T.; Krivanek, O. L. Temperature measurement by a nanoscale electron probe using energy gain and loss spectroscopy. *Phys. Rev. Lett.* **2018**, *120*, No. 095901.

(16) Dellby, N.; Bacon, N. J.; Hrncirik, P.; Murfitt, M. F.; Skone, G. S.; Szilagyi, Z. S.; Krivanek, O. L. Dedicated STEM for 200 to 40 keV operation. *Eur. Phys. J.: Appl. Phys.* **2011**, *54*, 33505.

(17) Bosman, M.; Keast, V. J.; Garcia-Munoz, J. L.; D'Alfonso, A. J.; Findlay, S. D.; Allen, L. J. Two-dimensional mapping of chemical information at atomic resolution. *Phys. Rev. Lett.* **2007**, *99*, No. 086102.

(18) Li, Y.; Wu, M.; Qi, R.; Li, N.; Sun, Y.; Shi, C.; Zhu, X.; Guo, J.; Yu, D.; Gao, P. Probing lattice vibrations at SiO2/Si surface and interface with nanometer resolution. *Chin. Phys. Lett.* **2019**, *36*, No. 026801.

(19) Varela, M.; Findlay, S. D.; Lupini, A. R.; Christen, H. M.; Borisevich, A. Y.; Dellby, N.; Krivanek, O. L.; Nellist, P. D.; Oxley, M. P.; Allen, L. J.; Pennycook, S. J. Spectroscopic imaging of single atoms within a bulk solid. *Phys. Rev. Lett.* **2004**, *92*, No. 095502.

(20) Li, G.; Cherqui, C.; Bigelow, N. W.; Duscher, G.; Straney, P. J.; Millstone, J. E.; Masiello, D. J.; Camden, J. P. Spatially mapping energy transfer from single plasmonic particles to semiconductor substrates via STEM/EELS. *Nano Lett.* **2015**, *15*, 3465−71.

(21) Wang, Z.; Santhanagopalan, D.; Zhang, W.; Wang, F.; Xin, H. L.; He, K.; Li, J.; Dudney, N.; Meng, Y. S. In situ STEM-EELS observation of nanoscale interfacial phenomena in all-solid-state batteries. *Nano Lett.* **2016**, *16*, 3760−7.

(22) Chang, Z.; Piligkos, S.; Møller, P. J. High-resolution electron-energy-loss spectroscopy of vanadium and vanadium oxide thin films on TiO2(110)−(1 × 1). *Phys. Rev. B: Condens. Matter Mater. Phys.* **2001**, *64*, 165410.

(23) Lagos, M. J.; Trugler, A.; Hohenester, U.; Batson, P. E. Mapping vibrational surface and bulk modes in a single nanocube. *Nature* **2017**, *543*, 529−532.

(24) Kliewer, K. L.; Fuchs, R. *Theory of Dynamical Properties of Dielectric Surfaces*; Wiley, 1974; Vol. *27*.

(25) Hohenester, U. Simulating electron energy loss spectroscopy with the MNPBEM toolbox. *Comput. Phys. Commun.* **2014**, *185*, 1177−1187.

(26) Alfaro-Mozaz, F. J.; Alonso-Gonzalez, P.; Velez, S.; Dolado, I.; Autore, M.; Mastel, S.; Casanova, F.; Hueso, L. E.; Li, P.; Nikitin, A. Y.; Hillenbrand, R. Nanoimaging of resonating hyperbolic polaritons in linear boron nitride antennas. *Nat. Commun.* **2017**, *8*, 15624.

(27) Rossouw, D.; Couillard, M.; Vickery, J.; Kumacheva, E.; Botton, G. A. Multipolar plasmonic resonances in silver nanowire antennas imaged with a subnanometer electron probe. *Nano Lett.* **2011**, *11*, 1499−504.

(28) Ashley, E.; et al. Dispersion relations for non-radiative surface plamons on cylinders. *Surf. Sci.* **1974**, *41*, 615−618.

DOI: 10.1021/acs.nanolett.9b01350
Nano Lett. 2019, 19, 5070−5076

(29) Chassaing, P. M.; Demangeot, F.; Paillard, V.; Zwick, A.; Combe, N.; Pagès, C.; Kahn, M. L.; Maisonnat, A.; Chaudret, B. Surface optical phonons in cylindrical ZnO nanoparticles: dielectric effect of outer medium. *Journal of Physics: Conference Series* **2007**, *92*, No. 012165.
(30) Losquin, A.; Kociak, M. Link between cathodoluminescence and electron energy loss spectroscopy and the radiative and full electromagnetic local density of states. *ACS Photonics* **2015**, *2*, 1619−1627.
(31) Giles, A. J.; Dai, S.; Vurgaftman, I.; Hoffman, T.; Liu, S.; Lindsay, L.; Ellis, C. T.; Assefa, N.; Chatzakis, I.; Reinecke, T. L.; Tischler, J. G.; Fogler, M. M.; Edgar, J. H.; Basov, D. N.; Caldwell, J. D. Ultralow-loss polaritons in isotopically pure boron nitride. *Nat. Mater.* **2018**, *17*, 134−139.
(32) Yoxall, E.; Schnell, M.; Nikitin, A. Y.; Txoperena, O.; Woessner, A.; Lundeberg, M. B.; Casanova, F.; Hueso, L. E.; Koppens, F. H. L.; Hillenbrand, R. Direct observation of ultraslow hyperbolic polariton propagation with negative phase velocity. *Nat. Photonics* **2015**, *9*, 674−678.
(33) Ambrosio, A.; Tamagnone, M.; Chaudhary, K.; Jauregui, L. A.; Kim, P.; Wilson, W. L.; Capasso, F. Selective excitation and imaging of ultraslow phonon polaritons in thin hexagonal boron nitride crystals. *Light: Sci. Appl.* **2018**, *7*, 27.
(34) Fuchs, R. Theory of the optical properties of ionic crystal cubes. *Phys. Rev. B* **1975**, *11*, 1732−1740.
(35) Zhang, S.; Bao, K.; Halas, N. J.; Xu, H.; Nordlander, P. Substrate-induced Fano resonances of a plasmonic nanocube: a route to increased-sensitivity localized surface plasmon resonance sensors revealed. *Nano Lett.* **2011**, *11*, 1657−63.
(36) MALIS, T.; CHENG, S. C.; EGERTON, R. F. EELS log-ratio technique for specimen-thickness measurement in the TEM. *J. Electron Microsc. Tech.* **1988**, *8*, 193−200.
(37) Kröger, E. Berechnung der Energieverluste schneller Elektronen in dtinnen Schichten mit Retardierung. *Z. Phys. A: Hadrons Nucl.* **1968**, *216*, 115.

DOI: 10.1021/acs.nanolett.9b01350
Nano Lett. 2019, 19, 5070−5076